MNRAS 000, 1–5 (2017) Preprint 23 June 2017 Compiled using MNRAS LATEX style file v3.0

Evidence for a possible bimodal distribution of the nodal distances of the extreme trans-Neptunian objects: avoiding a trans-Plutonian planet or just plain bias?

C. de la Fuente Marcos⋆ and R. de la Fuente Marcos
Universidad Complutense de Madrid, Ciudad Universitaria, E-28040 Madrid, Spain

Accepted 2017 June 22. Received 2017 June 21; in original form 2017 May 3

ABSTRACT

It is a well-known fact that the presence of a massive perturber interacting with a population of minor bodies following very eccentric orbits can strongly affect the distribution of their nodal distances. The details of this process have been explored numerically and its outcome confirmed observationally in the case of Jupiter, where a bimodal distribution of nodal distances of comets has been found. Here, we show evidence for a possible bimodal distribution of the nodal distances of the extreme trans-Neptunian objects (ETNOs) in the form of a previously unnoticed correlation between nodal distance and orbital inclination. This proposed correlation is unlikely to be the result of observational bias as data for both large semimajor axis Centaurs and comets fit well into the pattern found for the ETNOs, and all these populations are subjected to similar background perturbations when moving well away from the influence of the giant planets. The correlation found is better understood if these objects tend to avoid a putative planet with semimajor axis in the range 300–400 au.

Key words: methods: statistical – celestial mechanics – minor planets, asteroids: general – Oort Cloud – planets and satellites: detection – planets and satellites: general.

1 INTRODUCTION

Beyond the orbit of Neptune, but moving in regions mostly unaffected by Galactic tides, lies a population of minor bodies following very stretched elliptical paths. These large semimajor axis ($a > 150$ au) and long perihelion distance ($q > 30$ au) objects —the extreme trans-Neptunian objects or ETNOs (Trujillo & Sheppard 2014)— exhibit a number of unexpected orbital patterns that may be incompatible with the traditional eight-planets-only Solar system paradigm (see e.g. de la Fuente Marcos & de la Fuente Marcos 2014; Trujillo & Sheppard 2014; Batygin & Brown 2016a).

Peculiar orbital alignments can be caused by unseen massive perturbers in the framework of the trans-Plutonian planets hypothesis that predicts that one (Trujillo & Sheppard 2014; Batygin & Brown 2016a; Brown & Batygin 2016; Malhotra, Volk & Wang 2016; Millholland & Laughlin 2017) or more (de la Fuente Marcos & de la Fuente Marcos 2014, 2016a,b,c) yet-to-be-detected planetary bodies orbit the Sun well beyond Pluto. This interpretation has been received with skepticism by some members of the scientific community who argue that the currently available data are plagued with strong detection biases (Lawler et al. 2017; Shankman et al. 2017; Bannister et al. 2017); if observational biases are present, the data are inadequate to prove or disprove the presence of planets beyond Pluto. In stark contrast, a mostly negligible role of detection biases is advocated by Trujillo & Sheppard (2014), and by Batygin & Brown (2016a) and Brown & Batygin (2016). Although such biases obviously exist as discussed by e.g. de la Fuente Marcos & de la Fuente Marcos (2014), they do not seem to work quite in the way one would had hoped; for example, most discoveries should have low orbital inclinations, but this is not what is observed.

In the Solar system, Jupiter is the largest known perturber and a great deal can be learned about its impact on the orbital evolution of minor bodies following very elongated paths by investigating particular examples. In this context, de la Fuente Marcos, de la Fuente Marcos & Aarseth (2015) have studied the case of its gravitational relationship with comet 96P/Machholz 1 as a relevant dynamical analogue to understand better the behaviour of the ETNOs within the framework of the trans-Plutonian planets hypothesis. Their N-body simulations show that Jupiter can send minor bodies into high-inclination or even retrograde orbits and also eject them from the Solar system. Similar outcomes have been found within the context of the Planet Nine hypothesis (Batygin & Brown 2016b; de la Fuente Marcos, de la Fuente Marcos & Aarseth 2016).

However, Jupiter can affect the orbital architecture of the populations of minor bodies moving in highly eccentric paths in far more subtle ways. Rickman, Valsecchi & Froeschlé (2001) used numerical simulations to show that the values of the nodal distances of comets with $a < 1\,000$ au should follow a bimodal distribution. Here, we investigate the existence of a possible bimodal distribution of the nodal distances of the ETNOs. This Letter is organized

⋆ E-mail: nbplanet@ucm.es

as follows. Section 2 reviews the case of Jupiter and the comets with $a < 1\,000$ au. The case of the ETNOs is explored in Section 3. The analysis is further extended to large semimajor axis or extreme Centaurs and comets in Section 4. In Section 5, we study the statistical significance of our findings. Results are discussed in Section 6 and conclusions are summarized in Section 7.

2 JUPITER AND THE COMETS WITH a < 1 000 au

Rickman et al. (2001) investigated numerically the delivery of comets from the Oort cloud to the inner Solar system. In their fig. 6, they show that for comets captured in an orbit with $a < 1\,000$ au, the distribution of nodal distances (for the node closest to Jupiter's orbit), $r_{\rm n}$, should be bimodal with a primary peak near the present-day value of the semimajor axis of Jupiter (5.2 au) and a secondary peak in the neighbourhood of the Earth. For a direct or prograde elliptical orbit, the distance from the Sun to the nodes can be written as:

$$r_{\rm n} = \frac{a\,(1 - e^2)}{1 \pm e\cos\omega}\,, \tag{1}$$

where e is the eccentricity, ω is the argument of perihelion and the "+" sign is for the ascending node (where the orbit passes from South to North, crossing the ecliptic) and the "−" sign is for the descending node —for a retrograde orbit (inclination, $i > 90°$) the signs are switched. Rickman et al. (2001) showed that the primary peak is associated with captures due to close encounters with Jupiter while the secondary peak represents captures due to indirect perturbations because comets with short perihelion distances experience the largest perturbation as they speed up closer to the Sun. In addition, the strength of mean-motion resonances (in this case with Jupiter) is proportional to the eccentricity of the perturbed body (e.g. Nesvorný & Roig 2001).

As of 2017 June 5, the number of comets with $a < 1\,000$ au stands at 1 120 —here and in other sections, we use data provided by Jet Propulsion Laboratory's Solar System Dynamics Group Small-Body Database (JPL's SSDG SBDB, Giorgini 2011).[1] Fig. 1, bottom panel, is equivalent to fig. 6 in Rickman et al. (2001) but for real comets. In the histograms, we adopt Poisson statistics ($\sigma = \sqrt{n}$) to compute the error bars —applying the approximation given by Gehrels (1986) when $n < 21$, $\sigma \sim 1 + \sqrt{0.75 + n}$— and the bin width has been found using the Freedman-Diaconis rule (Freedman & Diaconis 1981), i.e. 2 IQR $n^{-1/3}$, where IQR is the interquartile range and n is the number of data points.

Using observational data, we confirm that the distribution of nodal distances is indeed bimodal. Fig. 1, top panel, is very similar to fig. 8, left-hand panel, in Rickman & Froeschlé (1988) that shows the distribution of nodal distances for short-period comets of the Jupiter family and includes both ascending and descending nodes. We observe that nodes tend to avoid the neighbourhood of the 3:2 and/or the 2:1 mean-motion resonances with Jupiter, but it is unclear why is this happening. These results are statistically significant ($> 8\sigma$) if we consider the associated Poisson uncertainties and they are unlikely to be affected by observational biases or completeness of the sample issues. Given this finding, it is not unreasonable to assume that massive perturbers, if present in the outer Solar system, should induce a similar behaviour on the populations of eccentric small bodies existing there.

[1] https://ssd.jpl.nasa.gov/sbdb.cgi

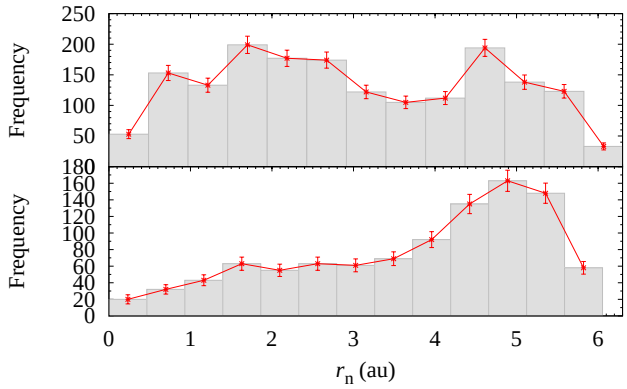

Figure 1. The distribution of the nodal distances of observed comets with $a < 1\,000$ au. Top panel, ascending and descending nodes (IQR=2.91 au, n=1 716); bottom panel, node closest to Jupiter (IQR=2.33 au, n=1 002).

3 A BIMODAL DISTRIBUTION FOR THE ETNOS?

As of 2017 June 5, the number of trans-Neptunian objects with $a > 150$ au and $q > 30$ au stands at 22 (see Table 1). It is therefore not advisable to try to produce a histogram similar to those in Fig. 1 only for this population. The uncertainties for 2003 SS_{422} and 2014 FE_{72} are the largest by far and the quality of their orbital solutions does not allow to reach any robust conclusion on the location of their nodes. The remaining data appear to be reasonably good and show that ascending nodes tend to be systematically located at barycentric distances < 200 au, which was expected as most objects in Table 1 have values of the argument of perihelion close to 0°. Surprisingly, the only examples of ETNOs with ascending nodes beyond 200 au correspond to the most uncertain orbits so their nominal locations may be incorrect (see Fig. 2 and Table 1).

Fig. 2 shows the distance to the descending node as a function of the distance to the ascending node of the ETNOs computed using barycentric elements (see Table 1). The distances have been calculated (averages and standard deviations, see e.g. Wall & Jenkins 2012) using 2 500 instances of the set of parameters a, e and ω for each object and applying Equation (1). For example, new values of a for a given ETNO have been found using the expression $\langle a\rangle + \sigma_a\, r_{\rm i}$, where $\langle a\rangle$ is the nominal value of the semimajor axis from Table 1, σ_a is its associated standard deviation, also from Table 1, and $r_{\rm i}$ is a (pseudo) random number with standard normal distribution. The Box-Muller method (Box & Muller 1958; Press et al. 2007) has been applied to generate the random numbers from a standard normal distribution with mean 0 and standard deviation 1. As 64 bits computers were used to complete the calculations, the smallest non-zero number is 2^{-64} and the Box-Muller method will not produce random variables more than 9.42 standard deviations from the mean. This fact should not have any adverse impact on our results, the standard deviations of the nodal distances in Table 1 are expected to be correct. Although it can be argued that the present orbital solutions of many ETNOs are too uncertain to use the data for this type of analysis, we believe that accounting for the role of the errors as we have done here greatly minimizes this issue.

In addition, Equation (1) shows that $r_{\rm n}$ does not depend on the orbital inclination and in absence of significant direct perturbations or resonances one may assume that the values of nodal distances and inclinations must be uncorrelated. Fig. 3 shows the orbital inclination as a function of the nodal distances for the same sample. Nodal distances in the range (200, 250) au seem to be avoided and the few present have associated values of the inclination within a

Table 1. Orbital elements (heliocentric and barycentric) and nodal distances of the ETNOs with 1σ uncertainties. Data include the heliocentric and barycentric semimajor axis, a and a_b, eccentricity, e and e_b, inclination, i and i_b, longitude of the ascending node, Ω and Ω_b, argument of perihelion, ω and ω_b, and their respective standard deviations, σ_a, σ_e, σ_i, σ_Ω and σ_ω; the computed heliocentric nodal distances, r_+ and r_-, and their barycentric counterparts, r_{b+} and r_{b-}, with their respective standard deviations (the "+" sign is for the ascending node and the "−" sign is for the descending node). The orbital solutions have been computed at epoch JD 2458000.5 that corresponds to 00:00:00.000 TDB on 2017 September 4, J2000.0 ecliptic and equinox. Source: JPL's SSDG SBDB.

Object	a (au)	σ_a (au)	a_b (au)	e	σ_e	e_b	i (°)	σ_i (°)	i_b (°)	Ω (°)	σ_Ω (°)	Ω_b (°)	ω (°)	σ_ω (°)	ω_b (°)	r_+ (au)	r_- (au)	r_{b+} (au)	r_{b-} (au)
82158	227.23	0.07	215.49	0.84914	0.00004	0.84106	30.762880	0.000053	30.800391	179.31043	0.00006	179.35869	7.1638	0.0011	6.8733	34.404±0.014	402.49±0.12	34.364±0.014	382.19±0.12
Sedna	487.77	0.62	507.42	0.84409	0.00021	0.84987	11.929003	0.000009	11.928559	144.45959	0.00147	144.40308	311.6130	0.0115	311.3066	89.864±0.169	319.13±0.52	90.275±0.166	320.99±0.51
148209	222.92	0.65	221.98	0.80139	0.00057	0.80123	22.756428	0.000585	22.755916	128.29160	0.00030	128.28584	317.0376	0.0117	316.6901	50.273±0.208	192.86±0.65	50.205±0.208	190.60±0.64
445473	150.48	0.02	153.43	0.77185	0.00004	0.77611	4.510987	0.000024	4.510524	117.39460	0.00147	117.39674	313.8822	0.0028	313.7247	39.629±0.009	130.83±0.03	39.710±0.009	131.62±0.02
474640	315.40	1.75	326.91	0.84999	0.00081	0.85525	25.592704	0.000317	25.547995	65.98210	0.00053	66.02214	326.9906	0.0093	326.9871	51.104±0.396	304.75±1.85	51.126±0.394	310.40±1.86
2002 GB_{32}	219.01	0.78	206.71	0.83860	0.00056	0.82903	14.175870	0.000310	14.192093	176.98897	0.00044	177.04362	37.1585	0.0047	37.0472	38.955±0.193	195.95±0.79	38.900±0.192	191.06±0.78
2003 HB_{57}	166.14	0.71	159.59	0.77061	0.00094	0.76128	15.472470	0.001354	15.500156	197.82250	0.00043	197.87105	11.0091	0.0631	10.8330	38.417±0.232	277.04±1.20	38.394±0.229	265.97±1.19
2003 SS_{422}	199.47	148.31	203.26	0.80296	0.16161	0.80657	16.811966	0.147140	16.781796	151.08067	0.17403	151.04186	211.7279	43.1730	211.5975	224±1733	42±69	227±1853	42±77
2005 RH_{52}	152.00	0.26	153.65	0.74365	0.00040	0.74620	20.445528	0.000718	20.446049	306.09328	0.00172	306.11117	32.3110	0.0619	32.5448	41.720±0.096	182.88±0.38	41.802±0.094	183.56±0.38
2007 TG_{422}	471.70	0.42	502.81	0.92462	0.00007	0.92927	18.603413	0.000075	18.595308	112.89216	0.00034	112.91072	285.6562	0.0034	285.6605	54.770±0.068	91.19±0.11	54.850±0.070	91.58±0.11
2007 VJ_{305}	188.02	0.16	192.17	0.81298	0.00016	0.81690	12.004643	0.000171	11.983580	24.38369	0.00008	24.38259	338.1883	0.0038	338.3541	36.331±0.045	259.98±0.24	36.337±0.044	265.59±0.23
2010 GB_{174}	363.66	25.46	351.38	0.86583	0.01021	0.86181	21.560511	0.005128	21.562666	130.71336	0.01973	130.71530	347.7672	0.3671	347.2366	49.311±5.080	591.81±42.26	49.119±5.091	566.85±42.17
2012 VP_{113}	255.76	1.34	262.07	0.68525	0.00195	0.69274	24.085640	0.002320	24.052058	90.73148	0.00562	90.80272	293.8367	0.3765	293.9250	106.24±0.89	187.62±1.64	106.41±0.88	189.56±1.66
2013 FS_{28}	196.70	98.78	191.76	0.82439	0.09765	0.82134	13.006215	0.024737	13.068231	204.67337	0.01617	204.63813	101.5395	2.4474	102.1765	75.47±55.58	54.10±41.92	75.47±53.68	53.18±39.62
2013 FT_{28}	312.28	10.53	294.52	0.86051	0.00505	0.85239	17.329026	0.003416	17.375249	217.78017	0.00483	217.72271	40.2649	0.1672	40.6969	48.92±2.47	236.02±9.87	48.92±2.46	227.65±9.62
2013 GP_{136}	154.27	0.82	149.71	0.73359	0.00168	0.72571	33.466607	0.001909	33.538942	210.70939	0.00023	210.72727	42.2113	0.1643	42.4635	46.16±0.37	156.02±1.04	46.16±0.37	152.52±1.04
2013 RF_{98}	349.23	11.73	363.87	0.89667	0.00358	0.90080	29.579219	0.003374	29.538373	67.58666	0.00532	67.63560	311.7287	0.6725	311.7566	42.86±2.04	169.77±8.07	42.89±2.07	171.49±8.07
2013 SY_{99}	672.89	21.43	729.24	0.92578	0.00245	0.93147	4.233857	0.001201	4.225428	29.47329	0.00519	29.50927	32.3248	0.1138	32.1410	53.96±2.46	441.81±17.31	53.96±2.50	456.82±17.79
2013 UH_{15}	170.66	8.30	173.75	0.79524	0.01131	0.79846	26.127110	0.005795	26.080631	176.60152	0.00721	176.54233	283.0936	0.2724	282.8653	53.16±3.74	76.52±5.12	53.47±3.75	76.60±5.09
2014 FE_{72}	1836.42	2066.40	1559.28	0.98020	0.02248	0.97680	20.616558	0.008942	20.637561	336.80375	0.01621	336.83831	134.3877	0.2131	133.9213	229±475	43±94	222±421	43±85
2014 SR_{349}	294.06	18.29	298.50	0.83813	0.01107	0.84073	17.984844	0.002072	17.968246	34.75185	0.01736	34.88438	341.2503	0.6557	341.2593	48.78±4.64	424.01±27.78	48.72±4.65	429.31±27.93
2015 SO_{20}	161.62	0.04	164.79	0.79481	0.00005	0.79871	23.451236	0.000136	23.410786	33.61877	0.00009	33.63407	354.8049	0.0063	354.8329	33.225±0.012	285.54±0.07	33.229±0.012	291.70±0.07

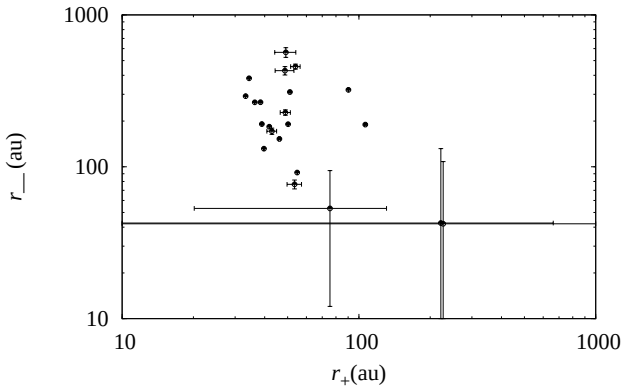

Figure 2. Distance to the descending node as a function of the distance to the ascending node for the 22 known ETNOs. The nodal distances have been found using the barycentric elements and the error bars have been computed using the uncertainties in Table 1 (see the text for details).

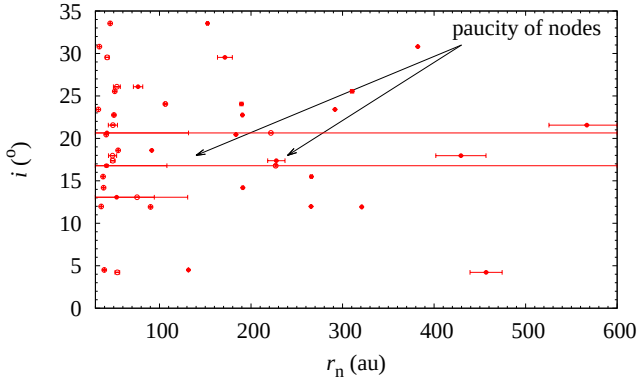

Figure 3. Orbital inclination as a function of the nodal distances. Nodal distances and error bars have been computed as in Fig. 2. Here and in Fig. 4, the arrows point out the regions where the paucities are located (see the text for details).

rather narrow range; a paucity of nodes in the range (100, 150) au does not show any obvious correlation with i. Although based on small-number statistics, the trend resembles that of the comets with $a < 1\,000$ au discussed in the previous section. If this correlation is real, it should also be observed among other populations that experience similar background perturbations during most of their orbital periods when moving well away from the influence of the giant planets. Such populations include the extreme Centaurs ($a > 150$ au but $q < 30$ au) and comets with $a > 150$ au and $e < 1$.

4 INCLUDING EXTREME CENTAURS AND COMETS

As of 2017 June 5, the number of extreme Centaurs stands at 24 although the orbits of three of them are rather poor (see Table 2); the number of comets with $a > 150$ au is 389. If we plot a figure analogue to Fig. 3 but including data for large semimajor axis Centaurs and comets with $a > 150$ au as well, we obtain Fig. 4 that shows that the extreme Centaurs follow the trend identified in the previous section. However, the distribution of the comets appears to be somewhat different as their overall inclinations are higher than those of ETNOs and extreme Centaurs; most comets have parameters outside the displayed range. This could be signalling a rather different dynamical origin for these comets when compared to ETNOs and extreme Centaurs. In Fig. 4, we have used heliocentric elements to compute the nodal distances applying Equation (1) as described in the previous section, but we have removed all the objects with relative errors in the value of the semimajor axis greater than 50 per cent (i.e. 2003 SS_{422}, 2014 FE_{72}, 2006 UL_{321}, 2012 KA_{51} and 2016 FL_{59} have not been included). The descending nodes of prograde extreme Centaurs tend to be systematically located near

Table 2. As Table 1 but for the known extreme Centaurs.

Object	a (au)	σ_a (au)	e	σ_e	i (°)	σ_i (°)	Ω (°)	σ_Ω (°)	ω (°)	σ_ω (°)	r_+ (au)	r_- (au)
87269	507.07	1.91	0.959083	0.000153	20.071069	0.000315	142.336335	0.000279	212.24223	0.00360	215.28±1.03	22.44±0.12
308933	785.55	0.94	0.969269	0.000037	19.498353	0.000056	197.341739	0.000094	122.27520	0.00068	98.54±0.16	31.33±0.05
336756	308.92	0.10	0.969570	0.000010	140.784619	0.000021	136.171903	0.000012	132.76335	0.00017	11.165±0.005	54.19±0.02
418993	355.27	0.11	0.969048	0.000009	68.079230	0.000015	220.222727	0.000014	128.61714	0.00008	54.79±0.02	13.492±0.006
468861	173.49	0.16	0.949692	0.000045	125.361075	0.000093	276.009114	0.000163	153.18391	0.00201	9.211±0.012	111.63±0.12
469750	170.92	0.06	0.828927	0.000063	6.189265	0.000186	192.460952	0.000540	227.99820	0.00242	120.09±0.05	34.40±0.02
1996 PW	251.90	0.32	0.990001	0.000013	29.796991	0.000065	144.539029	0.000030	181.60094	0.00043	482.64±0.61	2.519±0.005
2002 RN_{109}	578.90	25.88	0.995329	0.000209	57.926426	0.004905	170.502698	0.000057	212.38942	0.00580	33.83±2.14	2.93±0.19
2005 VX_3	1103.63	240.08	0.996267	0.000812	112.273081	0.007645	255.317842	0.001722	196.49382	0.01034	4.21±1.31	183.86±54.79
2006 UL_{321}	260.76	–	0.909904	–	37.366730	–	342.920200	–	353.79724	–	23.56	470.23
2007 DA_{61}	495.17	64.93	0.994602	0.000707	76.767820	0.009274	145.880900	0.002377	349.75417	0.01251	2.69±0.49	250.80±40.53
2010 BK_{118}	432.62	0.30	0.985917	0.000010	143.913110	0.000023	176.002953	0.000021	178.93966	0.00011	6.093±0.006	848.97±0.59
2010 GW_{147}	166.15	0.38	0.967601	0.000073	99.718297	0.000088	313.305837	0.000169	50.05406	0.00167	27.97±0.09	6.53±0.02
2011 OR_{17}	256.88	0.13	0.987921	0.000006	110.442034	0.000026	271.490201	0.000036	13.97512	0.00011	149.28±0.10	3.149±0.002
2012 DR_{30}	1595.55	3.72	0.990873	0.000021	77.966456	0.000046	341.415546	0.000023	195.53157	0.00029	639.86±1.88	14.83±0.05
2012 GU_{11}	183.93	0.07	0.900823	0.000036	10.751141	0.000041	144.788872	0.000234	6.55747	0.00101	18.298±0.010	330.00±0.12
2012 KA_{51}	224.45	2030.00	0.978126	0.197340	70.661491	0.251860	344.953286	0.484370	95.03797	5.57050	11±906	9±754
2013 AZ_{60}	562.45	0.36	0.985918	0.000009	16.531904	0.000014	349.201540	0.000028	158.41894	0.00006	189.06±0.16	8.206±0.007
2013 BL_{76}	1080.07	2.77	0.992258	0.000020	98.613012	0.000053	180.196765	0.000012	165.95965	0.00042	8.49±0.03	445.61±1.45
2014 GR_{53}	221.56	0.12	0.897855	0.000053	41.992112	0.000190	52.559667	0.000087	177.79558	0.00096	417.77±0.22	22.64±0.02
2014 LM_{28}	268.41	0.76	0.937525	0.000183	84.747713	0.000632	246.186279	0.000172	38.26251	0.03407	18.71±0.08	123.13±0.48
2015 FK_{37}	189.38	65.90	0.973867	0.009071	156.048232	0.025643	171.942377	0.021302	318.31574	0.10158	35.82±17.18	5.66±2.84
2016 FL_{59}	1237.17	124630.00	0.983370	1.684900	6.920160	0.002326	275.051954	2.225600	1.48279	23.42600	21±550770	2406±8061163
2017 CW_{32}	185.64	0.25	0.984069	0.000021	152.435852	0.000054	332.607656	0.000052	180.77294	0.00015	2.958±0.006	366.27±0.50

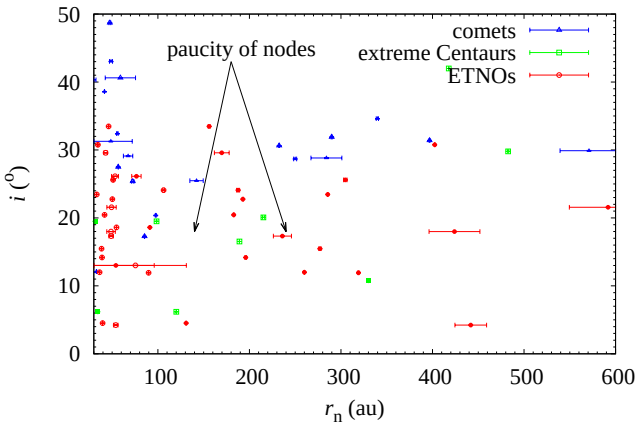

Figure 4. Orbital inclination as a function of the nodal distances for ETNOs (red circles, empty is r_-), extreme Centaurs (green squares, empty is r_-) and comets (blue triangles, empty is r_-). Nodal distances and error bars have been computed using heliocentric elements and uncertainties from Table 1.

perihelion as expected of objects with argument of perihelion preferentially close to 180° (see Table 2); this is exactly opposite to the trend observed for the ETNOs. Many extreme Centaurs follow orbits nearly perpendicular to the ecliptic (see Table 2, this is why they do not appear in Fig. 4), which is one of the evolutionary tracks predicted by numerical simulations when a massive perturber is present (de la Fuente Marcos et al. 2015, 2016; Batygin & Brown 2016b; Brown & Batygin 2016). Some extreme Centaurs may be former ETNOs. However, the orbital diffusion scenario recently advocated by Bannister et al. (2017) may not be able to reproduce this evolutionary track.

5 STATISTICAL SIGNIFICANCE

In the previous two sections, we have pointed out an interesting trend that is followed by both ETNOs and extreme Centaurs, that nodal distances in the range (200, 250) au seem to be avoided and the few present have associated values of the inclination within a rather narrow range. This trend means that the distribution of the nodal distances of the ETNOs (and the extreme Centaurs) could be bimodal. This tentative conclusion is based on data for 41 objects (20 ETNOs and 21 extreme Centaurs) as those with the poorest orbital solutions have been excluded from the analysis. This proposed correlation is unlikely to be the result of observational bias as the objects have been discovered by independent surveys, particularly the extreme Centaurs. If, as in the case of Jupiter, a 3:2 mean motion resonance (now, with an unseen perturber) is being avoided by the nodes of the orbiting minor bodies, the value of the semimajor axis of the putative planet should be close to 300 au or nearly 360 au if the resonance to be avoided is 2:1 instead of 3:2. If this interpretation is correct, nodal distances in the range 200–300 au must be scarce for a combination of the three eccentric populations.

Fig. 5 is equivalent to Fig. 1, bottom panel, but using data for ETNOs, extreme Centaurs and comets with $a > 150$ au; for a given object, only the node located farthest from the Sun has been counted. Although based on small-number statistics, the difference between the bin centred at 150 au and the one at 250 au is over 4σ; in addition, the excess of the bin centred at 350 au with respect to the one at 550 au is about 3.7σ —in both cases using the σ-value at the dip. In principle, this can be seen as an additional argument in support of our interpretation, if the dips are real. The second dip could be linked to a second perturber or perhaps both dips signal the nodes of a single perturber.

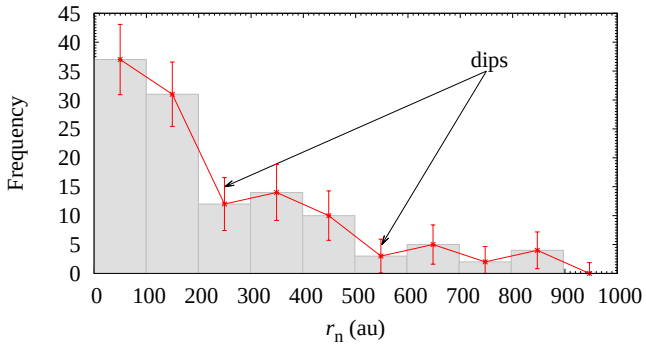

Figure 5. Similar to Fig. 1, bottom panel, but using data from Tables 1 and 2, and comets with $a > 150$ au (IQR=244.5 au, n=118). The arrows point out the bins where the dips are located (see the text for details).

6 DISCUSSION

Although the features pointed out in the previous section (and the associated bimodality in nodal distances) seem to be real, it can be disputed whether any dips present in Fig. 5 are nearly entirely due to lack of completeness of the sample or mainly due to observational biases. We believe that observational biases may not play a significant role in this case in light of the analysis performed on the nodal distance versus inclination correlation, but more data are needed to find out a definite answer to that question.

As for the presence of a planet at 300–400 au, the scenario explored by de León, de la Fuente Marcos, & de la Fuente Marcos (2017) also places that range in semimajor axis within the region of interest where a perturber may have been able to disrupt the pair of ETNOs (474640) 2004 VN_{112}–2013 RF_{98}, but only if its mass is in the range 10–20 $M_\oplus$. A closer perturber is also advocated by Holman & Payne (2016). Kenyon & Bromley (2015, 2016) have shown that super-Earths may form at 125–750 au from the Sun.

7 CONCLUSIONS

In this Letter, we have documented a previously unnoticed correlation between the nodal distances and the inclinations of the ETNOs. Although the size of the sample is small (22 ETNOs), the trend is also observed in other, perhaps related populations. The use of a dynamical analogy with Jupiter leads us to perform a tentative interpretation of our findings. Our conclusions are:

(i) The distribution of the nodal distances of observed comets with $a < 1\,000$ au is bimodal. This is a confirmation of results obtained by Rickman et al. (2001).

(ii) We found strong evidence for a possible bimodal distribution of the nodal distances of the ETNOs in the form of a correlation between their nodal distances and inclinations.

(iii) If the bimodal distribution in nodal distance observed in the case of Jupiter and those comets with $a < 1\,000$ au is used as a dynamical analogue for the ETNOs, one trans-Plutonian planet with semimajor axis in the range 300–400 au may exist. This result is consistent with the available data on both large semimajor axis Centaurs and comets.

ACKNOWLEDGEMENTS

We thank the anonymous referee for constructive, helpful, detailed and timely reports, S. J. Aarseth, J. de León, J.-M. Petit, M. T. Bannister, D. P. Whitmire, G. Carraro, E. Costa, D. Fabrycky, A. V. Tutukov, S. Mashchenko, S. Deen and J. Higley for comments on ETNOs and trans-Plutonian planets, and A. I. Gómez de Castro, I. Lizasoain and L. Hernández Yáñez of the Universidad Complutense de Madrid (UCM) for providing access to computing facilities. This work was partially supported by the Spanish 'Ministerio de Economía y Competitividad' (MINECO) under grant ESP2014-54243-R. Part of the calculations and the data analysis were completed on the EOLO cluster of the UCM, and we thank S. Cano Alsúa for his help during this stage. EOLO, the HPC of Climate Change of the International Campus of Excellence of Moncloa, is funded by the MECD and MICINN. This is a contribution to the CEI Moncloa. In preparation of this Letter, we made use of the NASA Astrophysics Data System, the ASTRO-PH e-print server, and the MPC data server.

REFERENCES

Bannister M. T. et al., 2017, AJ, 153, 262
Batygin K., Brown M. E., 2016a, AJ, 151, 22
Batygin K., Brown M. E., 2016b, ApJ, 833, L3
Box G. E. P., Muller M. E., 1958, Annals Math. Stat., 29, 610
Brown M. E., Batygin K., 2016, ApJ, 824, L23
de la Fuente Marcos C., de la Fuente Marcos R., 2014, MNRAS, 443, L59
de la Fuente Marcos C., de la Fuente Marcos R., 2016a, MNRAS, 459, L66
de la Fuente Marcos C., de la Fuente Marcos R., 2016b, MNRAS, 460, L64
de la Fuente Marcos C., de la Fuente Marcos R., 2016c, MNRAS, 462, 1972
de la Fuente Marcos C., de la Fuente Marcos R., Aarseth S. J., 2015, MNRAS, 446, 1867
de la Fuente Marcos C., de la Fuente Marcos R., Aarseth S. J., 2016, MNRAS, 460, L123
de León J., de la Fuente Marcos C., de la Fuente Marcos R., 2017, MNRAS, 467, L66
Freedman D., Diaconis P., 1981, Z. Wahrscheinlichkeitstheor. verwandte Geb., 57, 453
Gehrels N., 1986, ApJ, 303, 336
Giorgini J., 2011, in Capitaine N., ed., Proceedings of the Journées 2010 "Systèmes de référence spatio-temporels" (JSR2010): New challenges for reference systems and numerical standards in astronomy, Observatoire de Paris, Paris, p. 87
Holman M. J., Payne M. J., 2016, AJ, 152, 80
Kenyon S. J., Bromley B. C., 2015, ApJ, 806, 42
Kenyon S. J., Bromley B. C., 2016, ApJ, 825, 33
Lawler S. M., Shankman C., Kaib N., Bannister M. T., Gladman B., Kavelaars J. J., 2017, AJ, 153, 33
Malhotra R., Volk K., Wang X., 2016, ApJ, 824, L22
Millholland S., Laughlin G., 2017, AJ, 153, 91
Nesvorný D., Roig F., 2001, Icarus, 150, 104
Press W. H., Teukolsky S. A., Vetterling W. T., Flannery B. P., 2007, Numerical Recipes: The Art of Scientific Computing, 3rd edn. Cambridge Univ. Press, Cambridge
Rickman H., Froeschlé C., 1988, Celest. Mech., 43, 243
Rickman H., Valsecchi G. B., Froeschlé C., 2001, MNRAS, 325, 1303
Shankman C., Kavelaars J. J., Lawler S. M., Gladman B. J., Bannister M. T., 2017, AJ, 153, 63
Trujillo C. A., Sheppard S. S., 2014, Nature, 507, 471
Wall J. V., Jenkins C. R., 2012, Practical Statistics for Astronomers. Cambridge Univ. Press, Cambridge

This paper has been typeset from a TEX/LATEX file prepared by the author.